149 GRANT
IN-92-CR
130527
P- 51

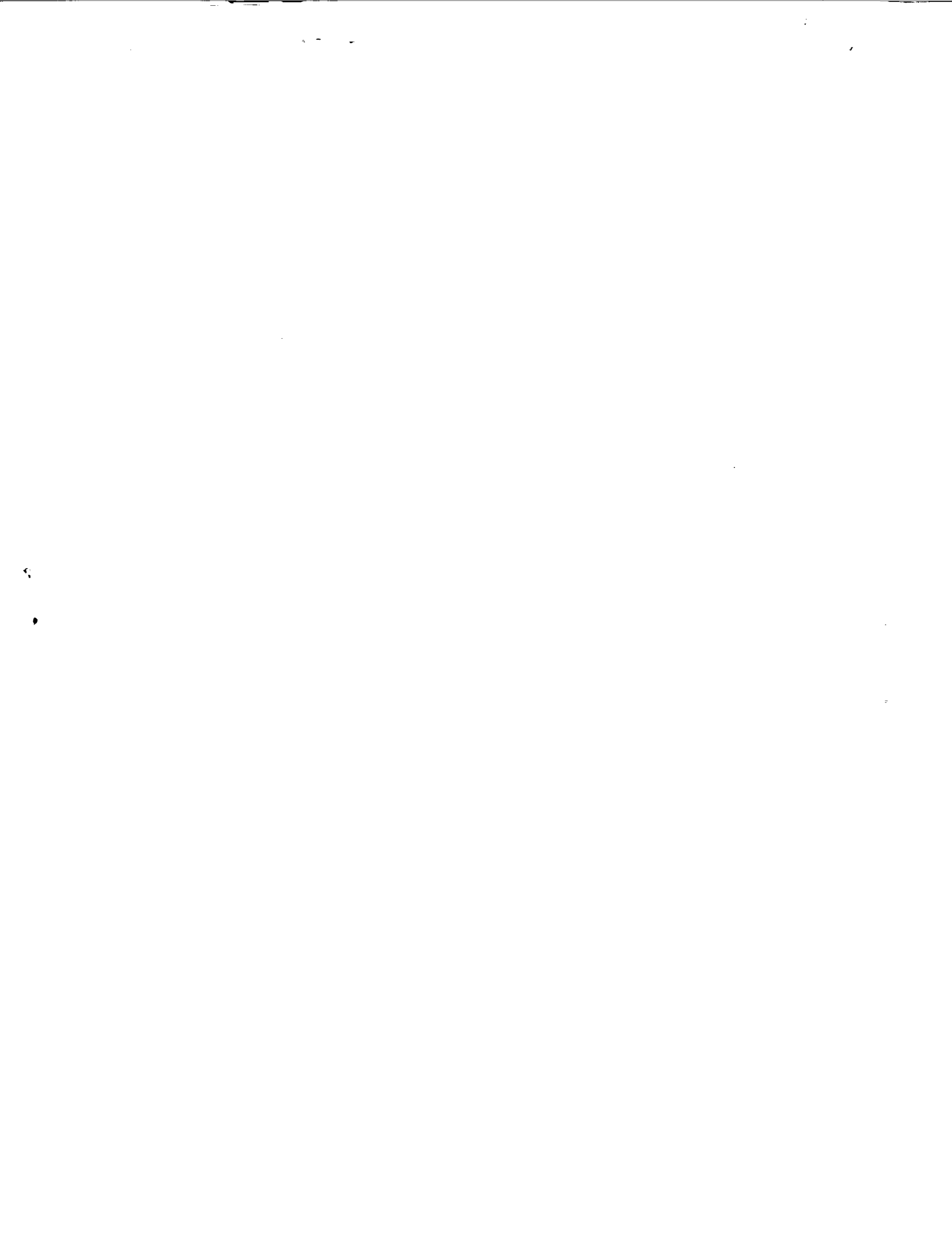|	
GRANT TITLE	STUDY OF *SMM* FLARES IN GAMMA-RAYS AND NEUTRONS
TYPE OF REPORT	FINAL REPORT
PRINCIPAL INVESTIGATOR	PHILIP P. DUNPHY
CO-INVESTIGATOR	EDWARD L. CHUPP
PERIOD COVERED BY REPORT	NOVEMBER 1, 1991 TO OCTOBER 31, 1992
GRANTEE'S INSTITUTION	UNIVERSITY OF NEW HAMPSHIRE SPACE SCIENCE CENTER DURHAM, NH 03824 (603) 862-2000
GRANT NUMBER	NAGW-2755

STUDY OF *SMM* FLARES IN GAMMA-RAYS AND NEUTRONS

1.0 INTRODUCTION

This report summarizes the results of the research supported by NASA grant NAGW-2755 and lists the papers and publications produced through the grant. The objective of the work was to study solar flares that produced observable signals from high-energy (> 10 MeV) γ-rays and neutrons in the Solar Maximum Mission (*SMM*) Gamma-Ray Spectrometer (GRS). In 3 of 4 flares that had been studied previously, most of the neutrons and neutral pions appear to have been produced after the "main" impulsive phase as determined from hard X-rays and γ-rays. We therefore proposed to analyze the timing of the high-energy radiation, and its implications for the acceleration, trapping, and transport of flare particles. Equally important was to characterize the spectral shapes of the interacting energetic electrons and protons – another key factor in constraining possible particle acceleration mechanisms. In Section 2.0, we discuss the goals of the research. In Section 3.0, we summarize the results of the research. In Section 4.0, we list the papers and publications produced under the grant. Preprints or reprints of the publications are attached as Appendices.

2.0 GOALS OF THE RESEARCH

Throughout the 10-year operating history of the *SMM* GRS, only a handful of solar flares have exhibited measurable emission of neutral pions (through pion-decay γ-rays) or high-energy neutrons (detected at the Earth). These radiations are of special interest, however, because they are direct evidence of the interaction of ions with energies $\gtrsim 50$ MeV at the Sun. The neutron spectrum is a direct probe of the interacting ion spectrum. The time history of the pion-decay γ-rays tracks the highest energy ions as they interact, and the intensity of these γ-rays are also sensitive to the ion spectrum when correlated with the intensity of γ-ray lines. No other observations, short of *in situ* measurements at the Sun, offer as clear a window to the non-thermal ion spectra near the solar surface.

Our research goal was to study the data from the High Energy Matrix (HEM) mode of the *SMM* GRS for large flares that showed evidence of ion acceleration (*i.e.*, neutral pion decay and high-energy neutrons). Previously,

1

two such flares had been analyzed and reported in detail, namely the flares of 1980 June 21 and 1982 June 3 (*cf.* Chupp (1990) for a summary). Two flares on 1988 December 16 and 1989 March 6 from the current cycle of solar activity have also produced neutrons sufficiently energetic and intense to be seen directly by the GRS (Dunphy *et al.* 1990; Dunphy and Chupp 1991).

It is noteworthy that, for 3 of the 4 flares in which neutrons have been detected by GRS, most of the neutrons and neutral pions appear to have been produced after the "main" impulsive phase as determined from hard X-rays and low-energy γ-rays. This may mean that the acceleration of protons to high energy , or, alternatively, the precipitation of trapped high-energy particles, in an "extended" or "delayed" phase may be a common feature of large flares. It may be significant that the flare which does *not* have this feature is a limb flare. Although it has not been recognized previously, the time history of the γ-ray emission during the delayed phase is also strikingly similar from flare to flare. This could be an important clue to ion acceleration in flares.

Our plans for this study were three-fold: 1) to search the *SMM* GRS data for additional flares that show the signature of pion-decay γ-rays or high-energy neutrons, 2) to analyze supporting data (*e.g.* γ-ray line emission, continuum emission, *etc.*) from the GRS (0.3 – 9 MeV) main channel, and 3) to evaluate models of flare particle acceleration and transport in light of the observed phenomena.

3.0 RESULTS OF THE RESEARCH

During the grant period, we have done preliminary analysis of the high-energy emission from the following flares: 1984 April 24, 1989 March 16, 1989 October 19, and 1989 September 29. In addition, we have done extensive analysis of the flares of 1989 March 7 and 1989 September 9. In order to study the proton spectrum for the flare of 1988 December 16, we have analyzed the nuclear line spectrum and its time variation. (The high-energy emission from this flare had already been reported by Dunphy *et al.* 1990.) Additionally, we have begun a detailed analysis of the shape of the π^0-decay spectrum from the flares of 1988 December 16 and 1989 March 6. A number of papers based on the grant work have been published or presented at conferences (see Section 4.0).

As an example of a preliminary analysis, we show in Figure 1 a time history

of the > 10 MeV emission from the 1984 April 24 flare observed by the GRS. The upper panel shows the time history of "multiple events" in the GRS HEM mode, which is sensitive primarily to > 25 MeV γ-rays. This channel shows a rapid onset and a decay that is characteristic of a number of flares that have produced measurable pion-decay and neutron emission. The lower panel shows the time history of the HEM "singles events," a mode which is more sensitive to solar flare *neutrons*. This channel shows enhanced emission (compared to the γ-rays) more than 10 minutes after flare onset, an effect that is due to the time-of-flight of the neutrons from the Sun to the Earth. This is clear evidence that the excess counts are due to neutrons. Unfortunately, the impulsive burst is so strong that the GRS suffered gain shift, dead time, and fold-over problems. This requires rather careful handling of the data analysis and, perhaps, exclusion of some of the data. This is especially true for the GRS "main channel" spectra in the 0.3 to 9 MeV energy range that contains the information on nuclear lines and is crucial (together with the high-energy data) for interpreting the flare proton spectral shape. Fortunately, the GRS does not have these problems at the time that most of the neutrons were detected. We expect to get useful results from further work on this flare.

Our analysis of the flare of 1988 December 16 has been published (Dunphy and Chupp 1992) and a reprint is attached as Appendix A. This work has the important result that the spectrum of protons interacting at the Sun, when the bulk of the high-energy emission was produced, was consistent with a Bessel-function shape over a broad energy range (from 10 MeV to over 300 MeV). This shape has been associated with stochastic acceleration mechanisms. The analysis also suggests that the proton velocity distribution was non-isotropic, based on theoretical calculations of the neutron and γ-ray yields for an isotropic distribution.

For the flare of 1989 September 9, we have participated in a multi-band study of the temporal evolution of the flare electrons and protons. The study took into account optical, radio, and X-ray, as well as γ-ray data. A key finding from this work was that variations in the X-ray and γ-ray emission were correlated with spatially (and temporally) distinct radio sources. This included an enhancement of emissions from protons relative to electrons (by a factor of $\sim$ 2) during a major burst that exhibited nuclear line emission and high-energy γ-rays above 10 MeV. This could be caused by a sudden increase in efficiency of proton acceleration compared to electron ac-

3

celeration. A paper reporting the results of this analysis has been submitted for publication (Chupp *et al.* 1992) and a preprint is attached as Appendix B.

During the grant period, we have begun a collaboration with theorists, Drs. David Alexander and Alexander MacKinnon, from the University of Glasgow. The focus of the collaboration is on the shape of the π^0–decay spectrum. Calculations have been done (Alexander and MacKinnon 1992) that show how the width of the π^0–decay feature (a broad peak near 70 MeV) depends on the proton spectrum above about 300 MeV. Therefore, this feature can be used as a probe of the proton spectrum up to very high energies. To this end, we are presently doing model–related fits of the π^0–decay peak using data from the flares of 1988 December 16 and 1989 March 6. The Principal Investigator and Co–Investigator were awarded a NATO Collaborative Research Grant to cover travel expenses for this work.

Finally, we have presented two papers at conferences. One was a review of significant measurements of high–energy neutrons during solar cycles 21 and 22 (Chupp and Dunphy 1991). The second paper discussed the importance of solar flare neutron monitoring in light of recent flare observations by detectors on the Compton Observatory (Chupp and Dunphy 1992).

4.0 PUBLICATIONS AND PAPERS PRESENTED

We list below, the titles and authors of the publications and papers produced under the grant. Reprints or preprints of the publications are included as Appendices.

"Solar Neutrons Detected in Space (1980–1989)," E. L. Chupp and P. P. Dunphy. Paper presented at the Fall Meeting of the American Geophysical Union, San Francisco, California, December 9–13 (1991).

"Gamma–Rays and Neutrons as a Probe of the Proton Spectrum During the Solar Flare of 1988 December 16," P. P. Dunphy and E. L. Chupp. Proceedings of the Particle Acceleration in Cosmic Plasmas Workshop, G. P. Zank and T. K. Gaisser, eds., AIP Conference Proceedings No. 246 (AIP: New York), p. 253 (1992).

"A Study of the Evolution of Electron and Ion Acceleration During the 09:09 Solar Flare on 1989 September 9," E. L. Chupp, G. Trottet, H.

Marschhäuser, M. Pick, I. Soru–Escaut, E. Rieger, and P. P. Dunphy. Submitted to Astronomy & Astrophysics (1992).

"Solar Flare Neutron Observations," E. L. Chupp and P. P. Dunphy. Paper presented at the COSPAR World Space Congress, Washington D. C., August 28 – Sept. 5 (1992).

5.0 OTHER REFERENCES

Alexander, D., and MacKinnon, A. L., 1992, submitted to *Astron. & Astrophys.*

Chupp, E. L., 1990, *Ap. J. (Suppl.)* **73**, 213.

Dunphy, P. P., Chupp, E. L., and Rieger, E., 1990, *Proc. 21st ICRC* **5**, 75.

Dunphy, P. P., Chupp, E. L., and Rieger, E., 1991, *Proc. 22nd ICRC* **3**, 65.
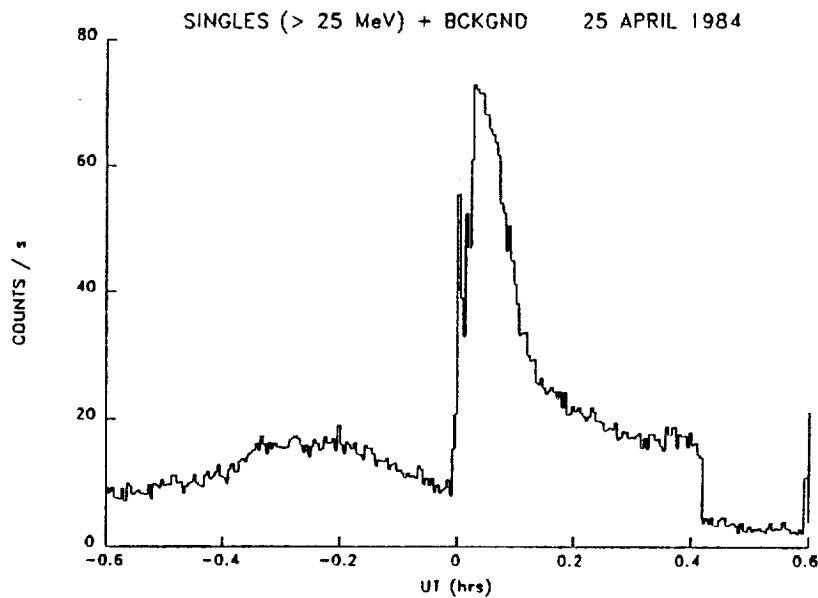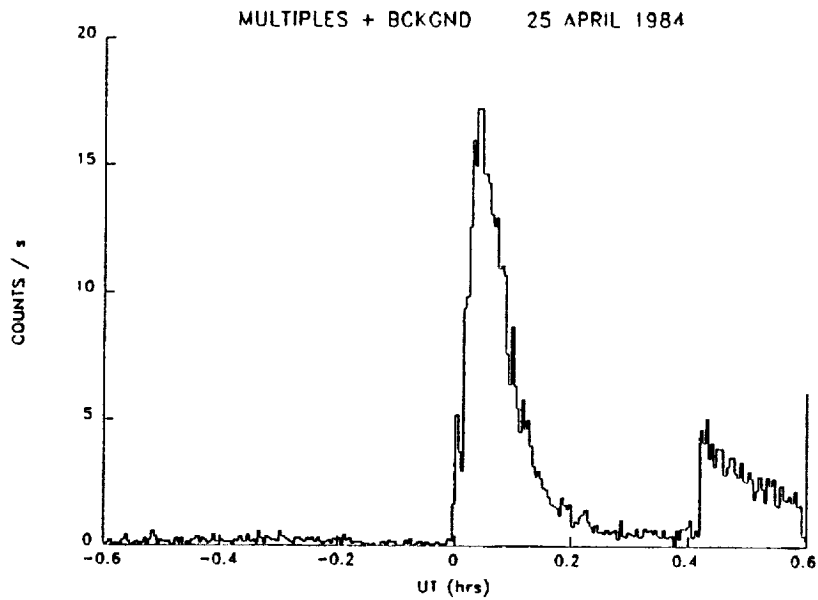
Figure 1. Upper panel: Time history of "multiple events" in the HEM mode of the GRS during the flare of 1984 April 24. This channel is most sensitive to high-energy γ-rays. The time scale is in hours measured from the time of flare onset. Lower panel: Time history of "singles events," a channel that is more sensitive to high-energy neutrons than the "multiple events" channel. The discontinuity near 0.4 hours is caused by the instrument going into a calibration mode at spacecraft sunset.

APPENDIX A

GAMMA-RAYS AND NEUTRONS AS A PROBE OF THE PROTON SPECTRUM DURING THE FLARE OF 1988 DECEMBER 16

GAMMA-RAYS AND NEUTRONS AS A PROBE OF THE PROTON SPECTRUM DURING THE SOLAR FLARE OF 1988 DECEMBER 16*

P. P. Dunphy and E. L. Chupp
Physics Department and Space Science Center
Institute for the Study of Earth, Oceans and Space
University of New Hampshire
Durham, New Hampshire 03824, USA

ABSTRACT

We have previously reported on high-energy (> 10 MeV) γ–rays and neutrons from the flare of 1988 December 16 detected by the Gamma–Ray Spectrometer on the SMM satellite.[1] In this paper, we present results on γ–ray lines seen by the same detector during this flare. Together, these measurements constitute a powerful probe of the proton spectrum (> 10 MeV) that produces the flare neutrals. Analysis of the data suggests a Bessel-function proton spectrum with a shape parameter (αT) of 0.054 ± 0.004 and the number of protons above 30 MeV equal to $(9.0 \pm 0.9) \times 10^{32}$. The number of neutrons detected from this flare is much smaller than what is predicted from an isotropic distribution of the protons, indicating that the distribution may be non-isotropic.

OBSERVATIONS

We report on the observation of low-energy (0.3–10 MeV) γ-rays and high-energy (>10 MeV) γ-rays and neutrons from the flare of 1988 December 16. We apply the results from model calculations to the data to evaluate the proton spectrum that produced the γ-rays and neutrons.

The high-energy data are from the *SMM* GRS High Energy Matrix (HEM).[2] This mode of the GRS treats the seven 7.6 cm $\times$ 7.6 cm NaI(Tl) "main channel" scintillators as one layer of a two-layer detector. The second layer is a 7.5 cm thick $\times$ 25 cm diameter CsI(Na) "back shield." The HEM records energy-loss events in the range 10–100 MeV in broad energy-loss channels ($\sim$20 MeV wide).

Active region 5278 produced an X4.7/1B flare on December 16 at $\sim$ 0830 UT. The flare was located at N27 E33 on the solar disk, corresponding to a heliocentric angle of 43°. Figure 1(a) shows the time history of the flare in the energy range 4.1–6.4 MeV, which is dominated by nuclear de-excitation line emission. Figure 1(b) shows the time history for "multiple" events in the HEM from the flare. The multiple events are "showering" events in both layers of the HEM and are produced primarily by γ-rays (> 25 MeV). The bulk of the high-energy γ-rays are produced in a peak that occurs well after ($\sim$ 7 minutes) the flare onset at lower energies.

Figure 1 in Dunphy et al. [1] showed a similar time history of the flare in the HEM for "singles" events (involving only one layer of the HEM). The emission that was seen to continue after the main peak is a signature of solar flare neutrons, delayed by their time of flight from the Sun.

Murphy et al. [3] have shown that the spectrum of solar flare protons can be evaluated by using the ratios of various γ-ray emissions, namely: (1) the line at 0.51 MeV from positron annihilation, (2) the line at 2.22 MeV from deuterium formation, (3) the emission between 4 and 7 MeV from nuclear de-excitation, and (4) the broad peak centered at 68 MeV from neutral pion (π^0) decay. The GRS main channel spectra were used to determine the fluences of the 0.51 MeV, 2.22 MeV, and 4-7 MeV photons.

Figure 2. Gamma-ray spectrum in the GRS HEM during the peak of high-energy (> 10 MeV) γ-ray emission. A significant "bump" due to π^0-decay photons is present. The smooth curves are fits to the continuum (including the data < 10 MeV, which are not shown), to the π^0-decay peak, and to the total spectrum.
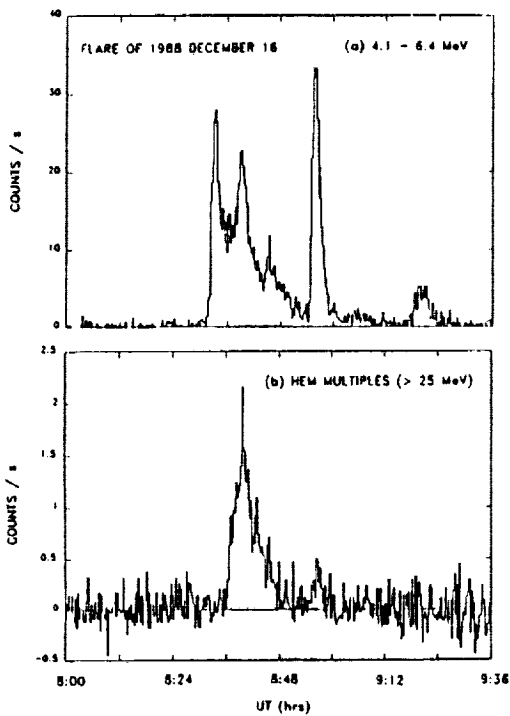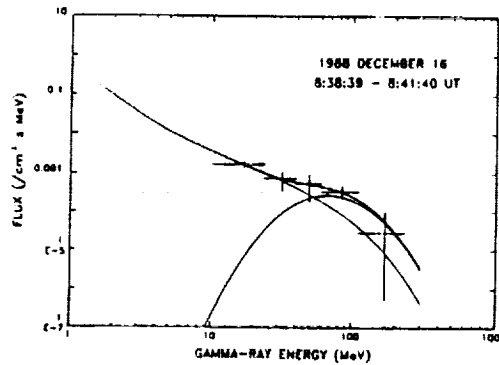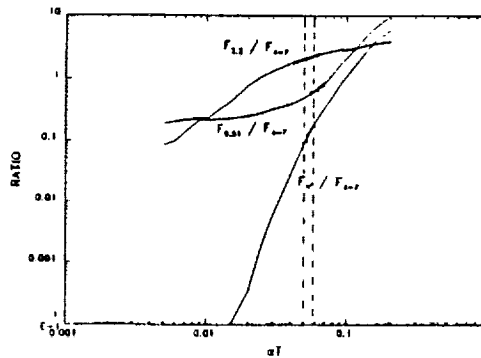

Figure 1. Time history of the 1988 December 16 flare in two GRS detector bands (background subtracted): (a) the 4.1-6.4 MeV band, sensitive to nuclear deexcitation γ-rays, and (b) the High Energy Matrix (HEM) multiple events, sensitive to γ-rays > 25 MeV.

Figure 3. The calculated dependence of γ-ray fluence ratios on the parameter αT for proton spectra with a Bessel-function shape.[4] The 1σ ranges in the ratios are indicated by the darkened sections of the curves. The corresponding range of αT (0.054±0.004) is also shown. The ratio $F_{2.2}/F_{4-7}$ depends on the heliocentric angle of the flare, which is 43°.

To determine the flux of the π^0-decay photons, we have used the GRS HEM data. In order to distinguish solar γ-rays from neutrons and to determine their energy spectra, we have developed an iterative fitting technique using the calculated response of the HEM. In principle, both the γ-ray and neutron fluxes can be determined independent of any model of the functional form for the differential energy spectra. In practice, the HEM response is not sensitive

enough to neutron energy to generate a stable, well-defined neutron energy spectrum unless the spectral shape is restricted. Therefore, we constrained the spectrum by assuming that all of the neutrons were produced at the Sun in a single, short time interval (*i.e.*, a δ-function production model). Figure 2 shows a γ-ray spectrum in the HEM for one 180 s time interval with strong emission above 10 MeV. The spectrum shows a significant feature due to π^0 decay.

RESULTS

The relationship between γ-ray yields and solar proton spectral shapes has been calculated by Murphy and Ramaty [4] for the case of isotropic production in a thick-target model of the interaction environment on the Sun. We have used their results to calculate the expected fluence ratios, normalized to the the fluence in the 4-7 MeV band. Figure 3 shows the dependence of these fluence ratios on the parameter αT that describes proton spectra with a Bessel function shape. Also shown in Figure 3 are the ratios for the December 16 flare. These ratios were determined for the time interval 08:36-08:48 UT during which there was significant flux from π^0 decay.

The observed ratios are consistent with a Bessel-function proton spectrum with a shape parameter (αT) equal to 0.054 ± 0.004. The measured fluences can then be used to calculate the intensity of the proton spectrum. In this case, the number of energetic protons above 30 MeV ($N_P > 30$ MeV) is $(9.0 \pm 0.9) \times 10^{32}$.

Although the γ-ray data are consistent with a Bessel function proton spectrum, they are *not* consistent with a single, unmodified power-law spectrum. (The data might be consistent with a modified power law – e.g., a power law with a high-energy cutoff.)
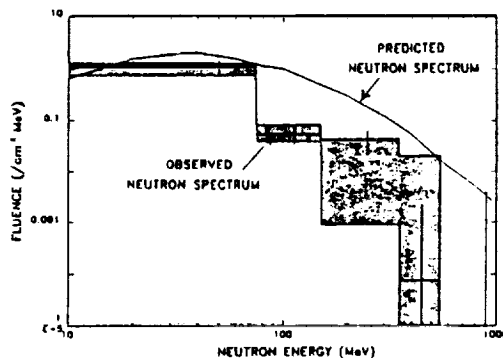

Figure 4. The time-integrated neutron spectrum observed by the GRS HEM, assuming δ-function neutron production at the time of peak γ-ray production > 10 MeV, is shown by the histogram. The shaded region encloses a range of spectra that depends on the range of assumed neutron production times (08:37-08:43 UT). The smooth curve is the neutron spectrum predicted from a Bessel-function proton spectrum interacting isotropically in a thick-target model.[5] The parameters of the proton spectrum, as determined from γ-ray line data, are $\alpha T = 0.05$ and N_P (> 30 MeV) = 9×10^{32}.

The proton spectrum calculated from the γ-ray data can be used to predict the neutron spectrum for the same isotropic thick-target model. We have used the neutron spectrum predicted by Murphy et al. [3] for a Bessel-function proton

spectrum with an αT of 0.05. This is shown in Figure 4 with the neutron spectrum observed by the GRS at 1 AU on December 16. In the range 10-75 MeV, the predicted fluence is reasonably close to the observed fluence, but above 75 MeV, the observed fluence falls below the predicted fluence by a factor of ~ 5. Since the predicted neutron spectrum does not account for γ-ray (and neutron) production outside the time interval 08:36-08:48 UT, the discrepancy is at least as large as is shown in Figure 4.

A similar analysis of the large 1989 March 6 flare [5] also showed an observed neutron spectrum that was below the predicted spectrum, in that case by a factor of ~ 2. It is important to determine whether these discrepancies are due to beaming effects, [6] since the present model assumes an isotropic distribution of energetic protons. Further observations of solar flare γ-rays and neutrons (for example, by the Compton Gamma Ray Observatory) would be valuable for such studies.

REFERENCES

1. Dunphy, P. P., Chupp, E. L., and Rieger, E., Proc. 21st Int. Cosmic Ray Conf. **5**, 75 (1990).
2. Forrest, D. J., et al., Sol. Phys. **65**, 15 (1980).
3. Murphy, R. J., Dermer, C. D., and Ramaty, R.,Ap. J. (Suppl.) **63**, 721, 1987.
4. Murphy, R. J., and Ramaty, R., Advances in Space Research (COSPAR) Vol. 4, No. 7, 127, 1985.
5. Dunphy, P. P., and Chupp, E. L., Proc. 22nd Int. Cosmic Ray Conf. **3**, 65 (1991).
6. Hua, X-M., and Lingenfelter, R. E., Ap. J. **323**, 779, 1987.

APPENDIX B

A STUDY OF THE EVOLUTION OF ELECTRON AND ION ACCELERATION DURING THE 09:09 SOLAR FLARE ON 1989 SEPTEMBER 9

A Study of the evolution of electron and ion acceleration during the 09:09 UT solar flare on 1989 September 9

Chupp, E.L.[1] Trottet, G.[2], Marschhäuser, H.[3], Pick, M.[2] Soru-Escaut, I.[4], Rieger, E.[3] and Dunphy, P.P.[2]

[1]University of New Hampshire,Physics Department and Space Science Center, Durham, NH 03824, USA

[2]Observatoire de Paris Section de Meudon, DASOP and CNRS –URA 324, F-92195 Meudon Principal, Cedex, France

[3]Max-Planck-Institute für extraterrestrische Physik, 8046 Garching, Germany

[4]Observatoire de Paris Section de Meudon, DASOP and CNRS –URA 326, F-92195 Meudon Principal, Cedex, France

Abstract. By use of radio, optical, X-ray and γ-ray observations we have studied the evolution of electron and ion acceleration during the 09:09 UT solar flare on 1989 September 9. The event is characterized by changes in the energetic photon spectrum as new radio sources appear. As the flare develops, in energetic photon emissions, the hard X-ray emission increases sporadically and low level nuclear line emission appears. At the time of initiation of the major increase in intensity of energetic photons, the power law bremsstrahlung spectrum hardens significantly and photons > 10 MeV are produced. During this increase the electron and proton interaction rates are enhanced, respectively, by factors of 6 and (11–16). This may indicate that proton acceleration became more efficient than the acceleration of electrons to relativistic energies. The increased efficiency in producing the energetic electrons and ions is clearly associated with the appearance of a new radio source. It is of particular interest that a new eruptive $H\alpha$ feature appears outside the main flare ribbons in association with the major phase of the flare.

1 Introduction

Radio studies and joint investigations of wide-band electromagnetic radiation have given new insight into the process of energetic electron production during solar flares. An understanding of the role of complex magnetic configurations in the flare energy release have been deduced from X-ray and radio imaging observations obtained with time resolutions better than 1 s. In particular, for impulsive events, Raoult *et al.* (1985) studied the durations and spatial characteristics of the hard X-ray and radio emissions. Their main conclusions were:

There is a close association between X-ray and Type III/V bursts, when the latter appears in the decimeter range, contrary to the case of dekameter observations.

Radio and hard X-ray fluxes have very similar durations, even though they are produced at different altitudes by different mechanisms.

The radio emission always presents a complex spatial structure. The most striking characteristic is that a *new source* systematically appears at the time of the rapid hard X-ray increase. This new source has the same time evolution as one of the previous sources which is at a different location. Raoult *et al.* (1985), proposed that the same population of electrons can account for the radio and X-ray emissions and later demonstrated the feasibility of this model by extensive calculations (Raoult *et al.* 1990). The temporal and spatial evolution of these two emissions can be explained by the interaction of two magnetic structures, the injection/energy release site being located in the region of interaction.

Nevertheless, these results suffered from some limitations in several ways:

Radioheliograph observations, whereas providing the major source of information for the understanding of the large scale magnetic topology, were limited to one frequency. This limitation is now removed with the availability of the new Nançay multifrequency radioheliograph.

In the absence of optical data, the identification of two magnetic structures interacting together can only be indirect which is the case for most of the studies published in the literature; however, for the present event excellent Hα photographs are available.

No detailed γ-ray observations were available at the time of these earlier studies and it was not possible to investigate whether or not the same scenario holds for higher photon energies. The flare studied in this paper was near the central solar meridian and produced several nuclear γ-ray lines.

In the present work an event having an impulsive phase, which reaches photon energies greater than 10 MeV is studied in detail by comparing optical, X-ray, γ-ray, and radioheliograph observations. The main goal of this study is to investigate the role of the magnetic structure and its time evolution for high-energy events in which there are both impulsive hard X-ray and γ-ray emissions.

2 Description of instrumentation

The high-energy photon observations were made with the Solar Maximum Mission *SMM* Gamma-Ray Spectrometer (GRS), and its auxiliary X-ray de-

tectors. This instrument is one of seven solar observing instruments on the *SMM* satellite which were continuously pointed toward the Sun. The GRS consists of seven 7.62×7.62 cm NaI(Tℓ) detectors backed by a thick (10 cm), CsI(Na) detector, which functioned both as a rear anticoincidence shield for the NaI detectors and a high-energy detector for energy losses > 10 MeV. These detectors were surrounded by a 4π steradian anticoincidence shield. The GRS provides high-resolution γ-ray energy-loss spectra, between 300 keV and 9 MeV from the NaI detectors accumulated every 16.384 s. High time resolution count accumulations are available at 64 ms and 2.048 s in energy windows (300–350) keV and (4.1–6.4) MeV, respectively. Wide band energy-loss spectra between 10 and 100 MeV from the combined set of the NaI and the thick CsI detectors are available at 2.048 s time resolution. In addition, two small (10 cm^2 area) X-ray spectrometers covering the energy range 14–199 keV, provided coincident spectra with the GRS spectra with 1.024 s time resolution. A full description of the *SMM* GRS may be found in Forrest *et al.* 1980.

The primary radio observations were made with the Nançay Radioheliograph (The Radioheliograph Group 1983, 1989). This instrument, referred to below as NRH, provides one dimensional images with circular polarization measurements in the east-west and south-north directions. The 1989 September 9 event was recorded with the Mark IV version, which can perform multifrequency observations with the south-north (SN) array at 5 frequencies between 150 MHz and 450 MHz.

During the 1989 September 9 event the SN frequencies available were 164 MHz, 236 MHz, 327 MHz, 408 MHz and 435 MHz. The spatial resolution of the SN array, which is inversely proportional to the frequency, was 3.8′ at 164 MHz and two images per second were recorded for each observing frequency. The east-west (EW) array operated at an observing frequency of 164 MHz. During the 1989 September 9 event the spatial resolution for the EW array was 1.6′ and 10 images per second were recorded. The EW and SN

one dimensional images allow us to obtain the 2-d postions of the centroids of the 164 MHz emitting sources, projected on the solar disk. At the other frequencies, for which only SN images are available, the projection on the solar disk of the actual position of the centroid of a given source lies along a straight line. The accuracy of absolute position measurements is about 0.2′ and 0.5′ for the EW and SN arrays, respectively.

For dynamic meterwave spectra, the Daedalus spectrometer at Zürich (courtesy of A.Benz) and the Weissenau spectrograph (courtesy of H.W. Urbarz) provided data. Additional meterwave and microwave intensity data at several discrete frequencies were provided by the US Air Force RSTN Stations at San Vito, Italy (courtesy of E. Cliver). Hα observations of the 1989 September 9 flare were made at the Paris–Meudon Observatory using the 3 λ Hα heliograph (Banos 1967) which consists of a 150 mm diameter telescope (f/14) equipped with a 0.5 Å Lyot filter. Whole solar disk images are recorded on a 35 mm film. Three successive images are taken within a cycle of 10 seconds, repeated every minute, in the Hα line center and in red and blue wings at + and − 0.5 Å respectively, from the line center. The exposure times are < 1 s and the spatial resolution is about 1.5″.

3 Description of event

The 1989 September 9 Hα1B (*GOES* X1) flare occurred in NOAA region 5680 (N18°, E28°), at 0908 UT (*GOES* 1–8 Å). See also Dennis *et al.* (1992). The associated radio emission reported by NOAA (Solar Geophysical Data) consists of microwave bursts and Type III/V and Type IV bursts at decimeter wavelengths. A Type II burst was also reported.

Figure 1 shows time histories of X-ray and γ-ray emissions at the highest time resolution from 09:08:00 UT to 09:13:00 UT which comprises, essentially,

the full event except for a long-duration thermal emission (see Figure 6) and decaying 2.223 MeV line emission. The different panels in the figure are the raw counts in the indicated energy bands. Typically, at energies below ~0.8 MeV the energy loss spectrum is due predominantly to electron bremsstrahlung and at the higher energies both bremsstrahlung and nuclear γ rays contribute.

The evolution of the radio emission during the event is displayed in Figure 2 which shows isointensity contours from the NRH at 327 MHz. Three radio sources are indicated on the figure which appear at different times as the event evolves.

We next describe the evolution of the radio, optical, and X- and γ-ray emissions in three different time intervals in which distinctive radio features appear.

3.1   *(09:08:17–09:09:30) UT*

The flare is first evident in soft X rays (14–21 keV), starting at about 09:08:17 UT. The initiation time of the event in several different GRS photon energy bands are shown in Table 1 using data of the highest time resolution for each band. The values given correspond to the range of times for which the increase of counts is typically 2 σ above the preceding background. The meterwave emission starts between 09:09:20 UT and 09:09:30 UT at all five NRH observing frequencies. As shown in Figure 2, at 327 MHz the emission arises from a source marked S1.

A more graphic illustration of the location of the radio sources is obtained by projecting the NRH locations onto the solar disk. Figure 3a shows these positions for the radio emitting sources at 164 and 327 MHz, just before onset of the hard X-ray burst (114–199) keV at ~ 09:09:32 UT. The 327 MHz

emitting source lies along the line marked S1 which crosses the flaring active region marked F. This suggests that S1 is overlying the flaring site F. This is consistent with the location of the corresponding source at 164 MHz (marked + on Figure 3a), the projection of which is in the vicinity of F but somewhat farther than S1 from F as is expected because the altitude of radio emitting sources increases with decreasing frequency. Within the spatial resolution of the NRH the 408 and 435 MHz emitting sources are also located along S1 while at 236 MHz the emission arises from a region (not shown on the figure), located along a line parallel to S1 which lies between S1 and +. The emission is 60–80% right hand circularly polarized at all frequencies.These properties are compatible with plasma emission at the fundamental of the local plasma frequency and the emission is like a noise storm emission (cf Kai, Melrose and Suzuki 1985). In addition to this noise storm like emission, short duration bursts (~1 s), identified as Type III bursts are also observed on the Daedalus spectrograph records. Their starting frequencies are lower than about 300 MHz and their locations at 164 MHz are marked by triangles (▲) on Figure 3a. It can be seen that the Type III bursts arise from sources at various locations close to and also remote from the flaring site F. Such an emission pattern is characteristic of the pre-flash radio emission often observed before the rapid increase of the hard X-ray flux (e.g., Benz et al. 1983; Raoult et al. 1985).

3.2   (09:09:30–09:10:34) UT

The hard X-ray emission (114–199) keV starts at 09:09:32 UT which is within 1 s of the appearance of a new radio source S2, shown in Figure 2. The new radio source appears at the five NRH observing frequencies. Figure 4, upper two panels, compares the light curves for hard X-ray (114–199) keV and microwave emission at 4995 MHz observed at San Vito. The two lower panels in Figure 4 show light curves for the new source S2 at 327 MHz and 435 MHz.

It is evident by comparison of the X-ray/γ-ray and radio light curves shown in Figure 4 that there is general correlation of the emission enhancements, but not a one-to-one correspondence between the times of occurrence of individual spikes. The reason for the lack of the detailed correlation is that the X-ray/γ-ray emission intensity is linearly related to the number of particles interacting in the solar atmosphere whereas the plasma radio emission processes are, generally, non-linear. The radio peak at 09:12:30 UT is not associated with the Type III/V emission but with a Type II burst (see Figure 2), which started between about 09:11 UT and 09:12 UT in the metric band (Solar Physical Data # 543, part 1). The position of S2 on the solar disk at 327 MHz is shown in Figure 3b. The location of the 236 MHz, 408 MHz, and 435 MHz sources are also along S2. The emission from S2 is unpolarized and comprises both a broad band Type V continuum and Type III like bursts. As was previously reported (e.g., Kane and Raoult 1981; Benz et al. 1983; Raoult et al. 1985) the starting frequency of the Type III bursts increases as the hard X-ray intensity increases (up to about 1000 MHz in the present case, A.O. Benz, personal communication). The two dimensional positions of these bursts, which are indicated by triangles ($\triangle$) on Figure 3b are spread around the S2 line. In this time interval S1 shows enhanced emission, but it was not possible to separate the relative contributions of Type III/V and storm like emission.

3.3 *(09:10:34–09:13:00) UT*

A very intense increase of the energetic photon intensity begins at 09:10:28 UT in all energy bands shown in Figure 1. It is remarkable that the *new radio source, S3*, appears at 09:10:34, but is observed only at 327 MHz in a band width < 172 MHz in contrast to the source S2 which was observed at the five NRH frequencies. Figure 5c shows that the time history of the intensity of S3 consists of a short duration and intense spike followed by a smoothly

decaying emission and a fainter spike just before 09:12 UT. A similar time behaviour is also observed for S2 but the intense spike and the subsequent emissions are stronger. It is important to notice in Figure 5c and 5d that the first peak in both sources S2 and S3 corresponds to the beginning of the rise in intensity of the (4.1–6.4) MeV and (10–25) MeV γ/ rays, while the second, S2, peak is associated with the peak γ-ray emission. The light curve of the Type II emission (which seems spatially near the source, S2, as shown in Figure 2) cannot be separated from the S2 light curve, as shown in Figure 5d. The projected position of the source, S3, is between the S1 and the S2 positions as shown on Figure 3. (The radio emission from S1 lasts much longer than the hard X-ray and γ-ray emissions. This noise stormlike emission, which corresponds to the dotted curves in Figure 6a and 6b, has an intensity/time evolution similar to the soft X rays shown in Figure 6c.)

3.4 $H\alpha$ observations

Figure 7 shows a time series of three $H\alpha$ images taken respectively in the blue wing(left strip), at the center (middle strip) and in the red wing (right strip) of the line. As explained in Section 2, successive triplets were obtained about every minute and we will subsequently use the time of the image taken in the line center as a reference. While the most intense portion of a flare is observed in the core of the $H\alpha$ line, the wings are also affected. This is especially evident in the flash stage, even for a weak flare (Ellison 1952). It should be noted that bright faculae are only observed in the line center. Therefore, because of contrast it is more difficult to detect the onset of a flaring feature in the center of the line than in the wings. Thus an emission seen also in at least one wing, determines accurately the initiation time of an $H\alpha$ flare. Detailed examination of the film reveals that the 1989 September 9 flare is first seen in both wings of the $H\alpha$ line within 1 minute of 09:09:06 UT. The emission intensity increases till about 09:12:20 UT and

remains thereafter nearly constant untill about 09:17 UT. From examination of Figure 7 we can emphasize the following points:

1. The Hα emission pattern consists of one quasi-circular ribbon surrounding the second ribbon (see frames at 09:10:11 UT and thereafter). The flare is thus initiated along a quasi circular neutral line between a North magnetic polarity which appeared in a facula of South polarity. This type of configuration has been described in detail by Mouradian *et al.* (1989) who indicate that the flare pattern consists of a collection of arches having one foot point in the parasitic north-polarity and the other foot point in the facula of opposite polarity, all around the $B_{\parallel}=0$ line. Such an unusual shape has been previously reported for one flare by Tang (1985). [N.B. The occurrence of Type III emissions (see Section 3.3) indicates that open magnetic structures are also involved in the flaring region.]

2. *A region (marked by an arrow in Figure 7)*, north-west of the two ribbons, shows an intensity increase in the center of the line which is first seen at 09:10:11 UT. This bright feature is clearly seen at 09:11:15 UT in both wings of the line. This indicates that an additional energy release probably occurred between 09:10 and 09:11 UT. This observation is similar to that reported by Wüsler *et al.* (1990) for 19:00 UT flare on 1989 March 10. Within this one minute time interval, the radio source S3 at 327 MHz appears and the hard-X-ray and gamma-ray flux strongly increases. *A causal association, between these optical, hard X-ray/γ-ray and radio features* is further supported by the fact that the new Hα flaring region and the new radio source S3 are both located to the north of the initial Hα flaring volume and the location of the initial initial radio source S1. It should be noted that a fainter Hα feature north of the main bright feature (marked by an arrow) is also visible at 09:11:15 in the center of the line and appears in the wings at

11

09:12:00 UT. This feature has no clear radio and/or hard X-ray/γ-ray counterpart except possibly the occurrence of the Type II radio burst.

3.5 *Hard X-ray/γ-ray spectral observations*

We describe the evolution of the hard X-ray and γ-ray spectra of the flare which commenced at 09:08:17 UT in the GRS energy band (14–21) keV. This was accomplished by a detailed analysis of the high resolution GRS spectra obtained in several successive 16.384 s time intervals throughout the flare.

Figure 8, (lower curve), shows the background subtracted GRS count spectrum, accumulated over the time interval (09:09:47—09:10:36) UT, during which the GRS first responded to emission above 300 keV. This interval corresponds to three 16.384 s spectral accumulations before the major burst accumulation is initiated at 09:10:36 UT. The spectrum consists of an apparent electron bremsstrahlung continuum and considerable line structure particularly above 0.8 MeV. It is interesting that the new radio source S2 appears at 09:09:30 UT, just before the start of this γ-ray spectral accumulation.

Using a direct inversion method (Marschhäuser 1992), this count spectrum has been deconvolved to give the net flare spectrum in photon space (Figure 9, lower curve). The net flare spectrum below 0.8 MeV was fit to a power law, which approximates the bremsstrahlung spectrum between 0.3 and 0.8 MeV. This power-law fit is then folded through the instrument response and plotted on the lower panel of Figure 8 as a solid line to compare with the measured count spectrum. In general, separation of the bremsstrahlung and nuclear contribution above 0.8 MeV, particularly for the (4–7) MeV energy band, has been accomplished by extrapolating this power law from the lower energies. The excess in the spectrum above the extrapolated power law is usually called the nuclear line excess. On the other

hand, it has been recently shown that the observed bremsstrahlung spectrum above 0.8 MeV may deviate greatly from the simple power law determined at the lower energies thereby effecting the estimate of the nuclear line excess (Rieger and Marschhäuser 1990; Marschhäuser, Rieger and Kanbach 1991). [For the present discussion this refinement is only important for the spectrum observed during the major frame accumulation, corresponding to the intense burst (09:10:36–09:10:52).] The first line in Table 2 shows the power-law fit for the first accumulation period and the nuclear excess fluence (photons cm^{-2}) for the energy bands (0.8–2) MeV and (4–7) MeV.

The background subtracted count and photon spectra are shown for the next accumulation interval (09:10:36–09:10:52), by the upper curves in Figures 8 and 9, respectively. The second line in Table 2 gives the power-law fit and nuclear excess fluences for this time interval and the corresponding information for the three later successive time intervals when prompt hard X-ray and γ-ray emission was detectable is shown on the next three lines.

The present analysis of the GRS spectra has not included a study of the 2.223 MeV time history, nor the spectra of the emissions above 10 MeV. This analysis, while not directly related to the present study, will be treated in a forthcoming paper.

4   Discussion

Several conclusions, can be drawn from the radio and Hard X-ray/γ-ray obervations reported in the previous section. First, we confirm the following results:

1. The γ ray and radio emissions, though they arise from sources at very distant locations, switch on and off nearly simultaneously. This indicates that both kinds of emissions result from particles produced by a

13

common accelerator (*e.g.*, Klein *et al.* 1983; Raoult *et al.* 1985; Trottet 1986).

2. The appearance of new radio emitting sources in the corona is nearly coincident in time with increased efficiency of the particle production. This has been previously observed by Raoult *et al.* (1985) and Willson *et al.* (1990) in comparing hard X-ray and radio emissions. A similar phenomenon has also been detected on ~ 30 keV X-ray images (Hernandez *et al.* 1986; Machado *et al.* 1988). This may be interpreted as a signature of interacting loops, or an ensemble of loops, or as the result of rapid changes in the equilibrium state of the loops themselves, leading to explosive release of energy. In any case, it reflects rapid changes in the topology of the flare and the associated magnetic field driven, for example, by the emergence of new magnetic fluxes and/or by enhanced foot point motion or magnetic shears (*e.g.*, reviews by Hagyard 1990; Martin 1990; Moore 1990 and references therein).

Second, the present observations of the 1989 September 9 event enable us to examine, for the first time, the relationship between particle acceleration and rapid disturbances of the magnetic structures involved as inferred from radio and optical obsrvations. It has been observed in this event that the initiation of the hard X rays (>114 keV) at ~09:09:32 (Table 1), was associated closely with the appearance of a new radio source S2. There was no detectable excess radiation above 300 keV until about 20 s later indicating that the electron bremsstrahlung becomes harder before the main burst which was initiated at ~09:10:36. Also, as shown by the GRS spectrum in Figure 8 (lower curve) in the time interval 09:09:47–09:10:36 there is clear evidence for nuclear lines before the main burst.[1] The deconvolved photon spectrum for this time interval (Figure 9, lower curve) clearly shows signif-

---

[1]There are not sufficient counts in the 16.384 s subintervals to give a more precise time of initiation of nuclear line production.

icant line features at ~1.37 MeV, 1.67 MeV, 2.22 MeV, and 3.2 MeV with spectral structure above 4 MeV, suggesting a canonical nuclear line spectrum. Thus, the interaction of ions accelerated to at least several MeV was, in effect, detectable well before the main burst of γ rays. During the succeeding time interval 09:10:36–09:10:52 a fully developed nuclear line spectrum is evident as shown in Figures 8 and 9 (upper curves). A full analysis of the nuclear line spectrum is beyond the scope of this paper, however, it is interesting to note that the line at ~3.2 MeV, most likely from ^{20}Ne (Ramaty *et al.* 1979), is not easily identified in most flares as in the present case. In the present analysis the bin widths were selected with consideration of statistical limitations. Also, in the upper curves for Figures 8 and 9 we identify only the source of the strongest features in the energy band (0.8–2.0) MeV.

The ratio of fluences in the standard nuclear excess window (4–7) MeV to that in the (0.8–2) MeV window is the same within error (~0.45), as shown in the last column of Table 2 for the initial and main burst accumulations. This same ratio is found in other nuclear line flares (Marschhäuser 1992). After the main burst this ratio falls, presumably, because the Compton tail of the delayed 2.223 MeV photons, scattered in the photosphere, is contributing relatively more counts, as the prompt γ-ray lines are decreasing rapidly in intensity. The clear appearance of nuclear lines before the main γ-ray burst has not, to the best of our knowledege, been reported previously. The combination of flare location ($\theta c \simeq 30°$) and the fact that the emission is more significant statistically in the lower energy band probably made it possible for this feature of γ-ray line flares to be detectable. This observation does not contradict the picture that relativistic electron and ion acceleration can occur together (Forrest and Chupp 1984) but the combination of circumstances show, it can be detected at lower levels and before the intense burst of γ rays

which is usually assumed to be the initiation of γ-ray line production.

To provide quantitative information we derive the primary energetic particle spectra at the Sun. In this paper we use the ratio of the (4–7) MeV fluence to the 2.223 MeV line fluence, to determine the proton spectral shape, assuming, as an example, it is represented by a modified Bessel-function (*e.g.*, Hua and Lingenfelter 1987). This spectral form is characteristic of a stochastic acceleration process and is characterized by the parameter αT, where α is the acceleration efficiency and T is the mean time of escape from the acceleration region, or some damping time of the turbulence that accelerates the particles ((Forman *et al.* 1986, Ramaty *et al.* 1988)

The time integrated 2.223 MeV line fluence for this event is (32.8±1.3) photons cm^{-2}.[2] Then using the total (4–7) MeV fluence given in Table 2, we find $\mathcal{F}(2.223)/\mathcal{F}(4-7)=1.14\pm0.13$, which implies $\alpha T\sim0.017$ using the recent calculations of Hua and Lingenfelter (1987) for isotropic acceleration. Hua and Lingenfelter (1987) have also calculated the "proton number per unit fluence" of (4–7) MeV γ rays as a function of αT. Therefore, the total number of protons > 30 MeV and their interaction rates can be estimated for the different time intervals (assuming the proton spectral shape is constant with $\alpha T\sim0.02$), by multiplying the theoretical value by the appropriate measured (4–7) MeV or (2.223) MeV fluence. The results are given in Table 3. It is important to note that the value for the Bessel function spectral parameter derived here only describes a hypothetical proton spectrum which gives the total number of γ rays observed. If instead a power law is assumed for the primary energetic photon spectrum the fluence ratio given above gives a slope ~ -3.7 and an estimated number of protons >30 MeV $\sim1.4\times10^{32}$ compared with $\sim2.3\times10^{32}$ for the Bessel function case. The errors in the estimated

---

[2]This value is actually a lower limit to the 2.223 MeV line fluence and, in principle, must be corrected for the fraction of original line γ rays which are Compton scattered in the photosphere as discussed by Vestrand 1990. Since this theoretical correction factor depends on several unknown factors we do not consider it further in this analysis.

hypothetical particle numbers is ~20% for either spectral form.

The bremsstrahlung photon spectra were deduced by fitting a power law to the main channel GRS data as described above. The photon spectra given in Table 2 are then related to the electron spectra at the Sun by applying the procedure proposed by Bai (1977) and described in Murphy (1985). Table 4 displays electron spectra, total electron numbers, and interaction rates for the five intervals of time during the event.

The comparison between the numbers quoted in Tables 3 and 4 for the two first intervals of time, clearly demonstrates the sudden increase of the electron and proton interaction rates, respectively, by factors of about 6 and (11–16). The electron spectrum also becomes harder and the ratio of the number of > 30 MeV protons interacting to the number of > 1 MeV electrons interacting changes from $\sim 4 \times 10^{-2}$ to $\sim 10^{-1}$. If we assume, between the first two time intervals, that the relative enhancements of the interacting protons compared to the interacting electrons is a reflection of the accelerator properties, then we must conclude that the accelerator(s) is more efficient in increasing the γ-ray line producing protons than relativistic electrons.

After the main phase burst no additional radio source is observed and electron and proton interaction rates decrease to intermediate values, but the electron spectral index and the proton/electron ratio remains nearly constant in time. This indicates that the transport and storage of both protons and electrons are similar or that the characteristics of the accelerator do not vary much until the end of the event. The late peak in the 4.1–6.4 MeV emission corresponds to Interval 5 of time in Table 2, which shows that the mean interaction rate of protons during this interval is comparable to that obtained for the previous interval. As seen in Figure 6 the 327 MHz S4 source is also more active and produces a few bursts in the decreasing part of the

17

4.1–6.4 MeV emission. It should be noted that decimetric radio spikes are sometimes seen to follow the $\sim$ 30 keV X-ray emission (Güdel 1991).

Since radio sources are tracers of large scale magnetic structures in which electrons either propagate or are accelerated, these observations strongly suggest that the accelerator efficiency increases in producing more numerous and more energetic particles when the number of magnetic structures involved also increases. The near time coincidence between the appearance of an additional radio source and an increase in the hard X ray/γ ray emission in intensity and energy indicates that both phenomena are closely related. This is clearly demonstrated for the main burst, starting at $\sim$ 09:10:36 UT, which also gives rise to > 10 MeV photon emission and for which optical observations bring further information. (As mentioned earlier the > 10 MeV emission is mostly from electron bremsstrahlung.) The sharp onset of this peak is simultaneous with the switch on of the new radio source S3 at 327 MHz, which exhibits a short lived and very intense burst, followed by a fainter, but significant, radio emission which lasts about the same time as the 4.1–6.4 MeV emission. A bright Hα feature also appeared at the border of the two ribbons of the Hα flare around the time of the > 10 MeV peak.

The overall picture that can be drawn from the above discussion is, that particle acceleration and transport takes place in a complex magnetic field topology that undergoes rapid changes on time scales of tens of seconds and that the characteristics of the accelerator(s) is/are correlated in time with these changes.The appearance of the Hα feature erupting at the border of the two flare ribbons may be interpreted as the chromospheric signature of such magnetic changes and the switch on of the S3 327 MHz source as its coronal response. The Hα images are only taken every minute, so the appearance of the Hα feature may indeed precede that of S3 by at most 30 s. Taking 10^5 km as a typical height for S3, the magnetic disturbance propagates from the chromosphere to the corona with a mean velocity of $\sim$

3000 km/s. Assuming that the 327 MHz radio emission is at the fundamental of the local plasma frequency (and using a coronal density scale height of 10^5 km), the coronal region swept out by the perturbation has a mean density of$\sim 3 \times 10^9$ cm^{-3}. If the velocity is identified with the Alfvén velocity, we obtain a coronal magnetic field of ~ 75 G. Such a value is comparable to that derived by Mercier (1991) from measurements of the polarization of Type III bursts. Nevertheless, if the time delay between the Hα and radio features is substantially shorter than 30 s they are not causally related on Alfvènic time scales. Under these conditions one possible interpretation, is that the magnetic turbulence built up on Alfvènic time scales and not giving rise to an electromagnetic signature, leads, when it reaches a sufficient level, to energy release and particle acceleration in a region located between the Hα and 327 MHz levels. These electrons and protons are then responsible for both kinds of emissions. This is in agreement with the results of e.g., Kane and Benz (1986) and Güdel (1991), which on the basis of joint decimetric radio spike and HXR observations, indicates that the site of electron acceleration is located in the corona at densities ranging from $\sim 10^9$ to $\sim 10^{10}$ cm^{-3}.

5 Conclusions

The multi wavelength study of the 09:09 UT flare on 1989 September 9 has given further insight into the characteristics of the solar flare particle acceleration. The major results of the study show:

1. The appearance of new radio emitting sources in the corona is cosely associated in time with the time evolution of increased electron and ion production as reflected in changes in the spectra of hard X rays and nuclear γ rays. The times of occurrence of Hα brightenings also fit this scenario;

19

2. Gamma-ray line and neutron production is detectable before the major burst of energetic photons which also shows a cannonical γ-ray spectrum. Though this feature of a solar flare has not been previously reported it is consistent with the *SMM* discovery that electrons and γ-ray producing ions are accelerated together;

3. If the electron and ion interaction rates, throughout the event, reflect the properties of the acceleration mechanisms, then it must be concluded that the γ-ray producing ions are accelerated twice as efficiently as relativistic electrons during the major burst and

4. The density of the source region for the accelerated electrons and ions is about $10^9 - -10^{10}$ cm^{-3}.

Finally, we suggest that the results of the analysis of this event raise a new question about solar flares. Given that electron and ion acceleration is well developed, but at a low level in the early development of the flare, why is the number of interacting electrons and ions suddenly increased by an order of magnitude? One possible answer is that particles have been energized in a large complex volume in which they interact or from which they are immediately released. We expect that similar analysis of other flares, for which sufficient correlative data exists, will confirm and extend the results obtained for this flare.

Acknowledgements

Table 1.
GRS Initiation Time

Energy Band (keV)	Time (UT)
(14–21)	09:08:25-09:08:41
(114–199)	09:09:31–09:09:45
(300–350)	09:09:47–09:09:52
(4100–6400)	09:10:52–09:10:24

Table 2.
Bremsstrahlung spectra and nuclear line excess.

Time Interval (UT)	Power Law photons cm^{-2} MeV^{-1}	$\mathcal{F}(0.8-2.0)$ MeV photons cm^{-2}	$\mathcal{F}(4-7)$ MeV photons cm^{-2}	$\frac{\mathcal{F}(4-7)\text{MeV}}{\mathcal{F}(0.8-2)\text{MeV}}$
(1) 09:09:47–09:10:36	$4.4(\pm1.5)\,E^{-4.45(\pm0.21)}$	6.9±2.0	2.7±1.3	0.40±0.22
(2) 09:10:36–09:10:52	$32.0(\pm1.8)\,E^{-3.69.(\pm0.09)}$	28.9±5.0	14.9±2.4*	0.51±0.12
(3) 09:10:52–09:11:08	$13.6(\pm2.0)\,E^{-3.46(\pm0.20)}$	14.8±2.8	3.4±1.0	0.30±0.10
(4) 09:11:08–09:11:25	$9.6(\pm1.4)\,E^{-3.32(\pm0.11)}$	8.2±1.8	2.6±1.0	0.31±0.14
(5) 09:11:25–09:11:58	$12.2(\pm1.5)\,E^{-3.76(\pm0.02)}$	17.8±1.7	5.1±1.3	0.29±0.08

*If the power-law fit to the photon spectrum above 10 MeV, is extrapolated to < 10 MeV, this fluence value would be reduced by ∼ 26%.

Table 4

Electrons

Interval (UT)	Electron Spectrum (electrons MeV^{-1})	Total Number $N_e(> E_0$ MeV)	$I_e(> 1$ MeV) (electrons s^{-1})
(1)	$2.40 \times 10^{33} \, E^{-5.65}$	$5.16 \times 10^{32} \, E_0^{-4.65}$	1.1×10^{31}
(2)	$4.40 \times 10^{33} \, E^{-4.89}$	$1.13 \times 10^{33} \, E_0^{-3.89}$	6.9×10^{31}
(3)	$1.23 \times 10^{33} \, E^{-4.66}$	$3.36 \times 10^{32} \, E_0^{-3.66}$	2.0×10^{31}
(4)	$6.72 \times 10^{32} \, E^{-4.04}$	$2.21 \times 10^{32} \, E_0^{-3.04}$	1.3×10^{31}
(5)	$1.9 \times 10^{33} \, E^{-4.96}$	$4.80 \times 10^{32} \, E_0^{-3.96}$	1.5×10^{31}

Table 3.

Protons

Interval (UT)	Total Number $N_p(> 30$ MeV)	$I_p(> 30$ MeV) proton s^{-1}	$\frac{N_p(>30 \text{ MeV})}{N_e(>1 \text{ MeV})}$
(1)	2.2×10^{31}	$(4.5-6.7) \times 10^{29}$	0.04
(2)	1.2×10^{32}	7.3×10^{30}	0.1
(3)	2.7×10^{31}	1.6×10^{30}	0.08
(4)	2.1×10^{31}	1.3×10^{30}	0.1
(5)	4.1×10^{31}	1.25×10^{30}	0.08

References

Bai, T., 1977, Ph.D. Thesis, University of Maryland.

Banos, G., 1967, *Solar Physics* 1, 397.

Benz, A.O., Barrow, C.H., Dennis, B.R., Pick, M., Raoult, A., and Simnett, G., 1983, *Solar Physics* 83, 267.

Dennis, B.R., Licata, J.P. and Tolbert, A.K., *The 1989 Solar Maximum Mission Event Listing*, 1992, NASA TM4344.

Ellison, M.A. 1952, *Publication Roy. Obs. Edinburgh* 1, 75.

Forman, M.A., Ramaty, R., and Zweibel, E.G., 1986, in Physics of the Sun eds. P.A. Sturrock *et al.* (Reidel Publ. Co., Dordrecht, Holland), Vol. II, p. 249.

Forrest, D.J. and Chupp, E.L., 1983, *Nature* 305, 291.

Forrest, D.J.,*et al.* 1980, *Solar Phyics* 75, 15.

Güdel, M., 1991, Ph. D. Thesis *(Dissertation ETH no 9374)* p.176.

Hagyard, M.J., 1990, *J. of the Italian Astronomical Society* (ed. G. Poletto) 61, No. 2, p.337.

Hernandez, A.M., Machado, M.E., Vilmer, N., and Trottet, G., 1986, *Astronomy & Astrophysics* 167, 77.

Hua, X.M., and Lingenfelter R.E., 1987, *Solar Physics* 107, 351.

Hua, X.M., Ramaty, R., and Lingenfelter, R.E. 1989, *Astrophys. J.* 341, 516.

Kai, K., Melrose, D., and Suzuki, S., 1985, in *Solar Radio Physics* eds. McLean, D.J. and Labrun, N. (Cambridge University Press, Cambridge, England) p. 516.

Kane, S.R. and Raoult, A., 1981, *Astrophys. J. (Letters)* **248**, L77.

Kane, S.R. and Benz, A.O., 1986, *Solar Physics* **104**, 179.

Klein, K.-L., Anderson, K., Pick, M., Trottet, G., Vilmer, N., and Kane S.R., 1983, *Solar Physics* **84**, 295.

Machado, M.E., Moore, R.L., Hernandez, A., Rovira, M.G., Hagyard, M.J., and Smith J.B., 1988, *Astrophys. J.* **326**, 425.

Marschhäuser, H., Rieger, E., and Kanbach, G., 1991, *Proc. XXII Int. Cosmic Ray Conf.*, Dublin, Ireland, 1991, p. 61.

Marschhäuser, H., 1992, *Ph.D. Thesis* Ludwig Maximilian Universität, München.

Martin, S.F., 1990, *J. of the Italian Astronomical Society* (ed. G. Poletto) **61**, no. 2, p.293.

Mercier, C., 1990, *Solar Physics* **130**, 119.

Moore, R.L., 1990, *J. of the Italian Astronomical Society* (ed. G. Poletto) **61**, No. 2, p.317.

Mouradian, Z., Martres, M.J., Soru-Escaut, I., and Simnett, G., 1989, *Astronomy & Astrophysics* **224**, 267.

Murphy, R., 1985 *Ph.D. Thesis*, University of Maryland.

Ramaty, R., Kozlovsky, B. and Lingenfelter, R.E., 1979, *Astrophys. J. (Suppl. Series)* 40, 481.

Ramaty, R., Dennis, B.R., and Emslie, A.G., 1988, *Solar Physics* 118, 17.

Raoult, A., Pick, M., Dennis, B.R., and Kane, S.R., 1985, *Astrophys.J.* 299,1027.

Raoult A., Vlahos L., and Mangeney A., 1990, *Astronomy & Astrophys.* 233, 229.

Rieger, E. and Marschhäuser, 1990, in *Proceedings od MAX 91 Workshop* #3, eds. R.M. Winglee and A.L. Kiplinger (University of Colorado, Boulder) p. 68.

Tang, F., 1985, *Solar Physics* 102, 131.

The Radioheliograph Group, 1983, *Solar Physics* 88, 383.

The Radioheliograph Group, 1989, *Solar Physics* 120, 193.

Trottet, G., 1986, *Solar Physics* 104, 145.

Vestrand, W.T., 1990, *Astrophys. J.* 352, 353.

Willson, R.F., Klein, K.-L., Kerdraon, A., Lang K.R., and Trottet G., 1990, *Astrophys. J.* 357, 662.

Wülser, J.P. in *Proceedings od MAX 91 Workshop* #3, eds. R.M. Winglee and A.L. Kiplinger (University of Colorado, Boulder) p. 149.

Figure Captions

Figure 1. The time histories are shown for several X-ray and γ-ray energy bands from the *SMM* GRS during the 09:09 UT flare on 1989 September 9.

Figure 2. The Nançay Radioheliograph isointensity counts for the north-south array are shown for the meter-wave sources at 327 MHz as a function of time following the 09:09 UT flare on 1989 September 9. Three sources are indicated which begin at different times. The positions indicated by the NRH channel number are given in instrumental units (1 unit corresponds to about 0.07 solar radii).

Figure 3a. The location line for the polarized 327 MHz noise storm source is shown as S1 for the initial phase of the radio emission. The location of the Hα flare lying on the S1 line is indicated by F. The corresponding location of the 164 MHz source is shown by +. The solid triangles give the locations of Type III bursts observed by the NRH, at 164 MHz.

Figure 3b. A new radio source, S2 , appears at the onset of hard X-ray emission at 09:09:30 UT while the noise storm S1 continues. The corresponding location of the 164 MHz source is shown by an open triangle, indicated by the arrow. The location of Type III bursts associated with S2 are indicated by solid triangles. The location of the source S1 at 164 MHz is shown by a +.

Figure 3c. At 09:10:34 UT a new source S3 appears at 327 MHz, but not at other Nançay frequencies. The appearance of this source coincides with the major enhancement of hard X ray and γ ray intensity in the 4–7 MeV and >10 MeV ranges. The locations of sources S1 and S2 at 164 MHz are shown by + and an open triangle, respectively.

Figure 4. The time histories of the relative 327 MHz and 435 MHz intensities from the source S2 are shown in the upper curves of the two lower panels. The lower curves in the lower panels show the scaled polarization intensities. The hard X-ray (114–199) keV and microwaves time histories are shown in the upper two panels.

Figure 5. The time histories of the 327 MHz flux density are shown for the sources S2 and S3 with that for the γ-ray emissions above 4 MeV.

Figure 6 The emission from the source S1 at 327 MHz and 408 MHz are compared with the soft X-ray (14-21) keV intensity. The dotted curves in the middle and the upper panels correspond to the noise storm emission as estimated by taking the envelope below the burst.

Figure 7. The 1989 September 9 flare observed at the Paris-Meudon Observatory with the 3 λ heliograph. (Middle panel, Hα center; left panel, Hα; right panel, Hα+0.5Å)

Figure 8. (lower curve) The background subtracted counts spectrum from the *SMM* GRS is shown for the accumulation time interval (09:09:47-09:10:36) UT just before the main burst. Excess nuclear radiation emission is clearly evident in the energy channels corresponding to (0.8-2) MeV, 2.223 MeV, and 3.2 MeV.

(upper curve) The background subtracted counts spectrum from the *SMM* GRS is shown for the accumulation time interval (09:010:36-09:10:52) UT during the main burst. Excess nuclear radiation emission is clearly evident in the energy channels corresponding to (0.8-2) MeV, 2.223 MeV, and 3.2 MeV.

Figure 9. (lower curve) The deconvolved *SMM* GRS photon spectrum is shown for the time interval 09:09:47-09:10:36 UT during the 1989 September 9 flare. The straight line is a fit to the data below 0.8 MeV.

(upper curve) The deconvolved *SMM* GRS photon spectrum is shown for the time interval 09:10:36-09:10:52 UT during the 1989 September 9 flare. The straight line is a fit to the data below 0.8 MeV.
For both curves, the 1 σ error bars result from errors in the numerical inversion process and count statistics.
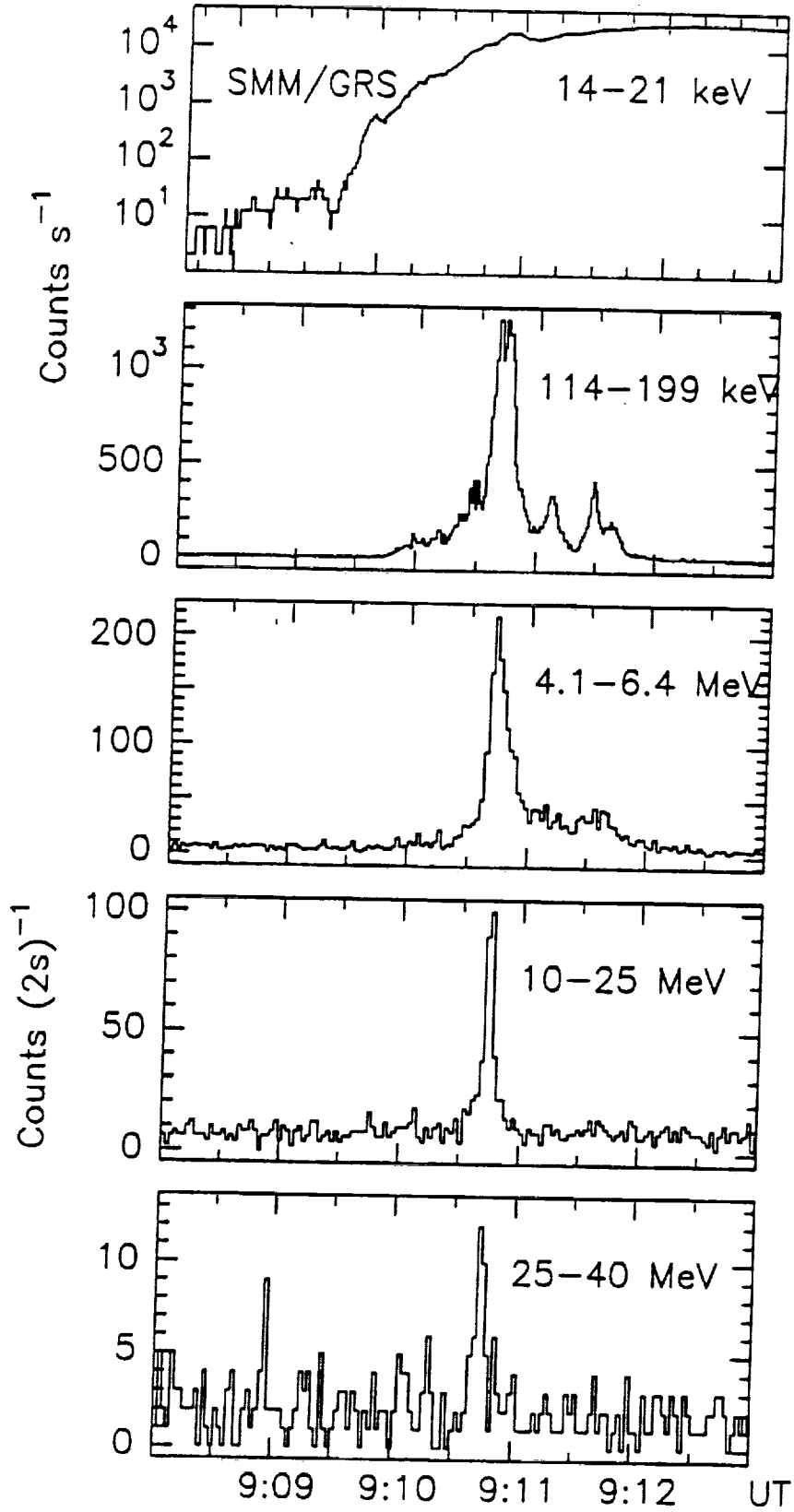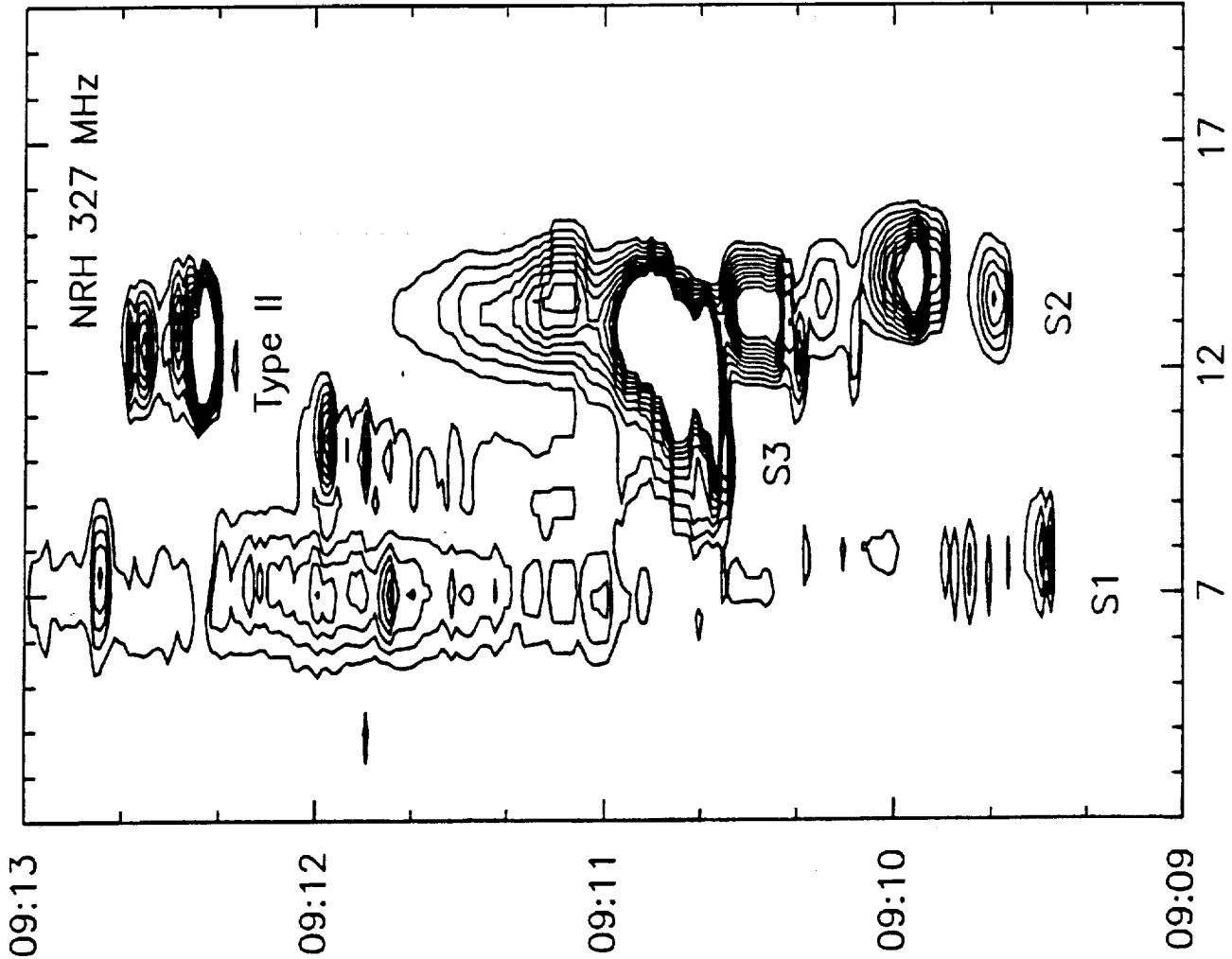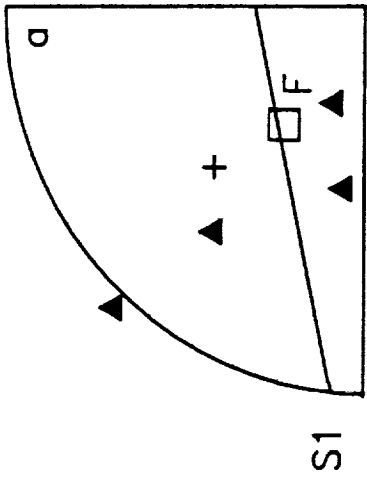
September 9,1989

SMM/GRS   14−21 keV

114−199 keV

4.1−6.4 MeV

10−25 MeV

25−40 MeV

Counts s⁻¹

Counts (2s)⁻¹

9:09   9:10   9:11   9:12   UT

FIGURE 1
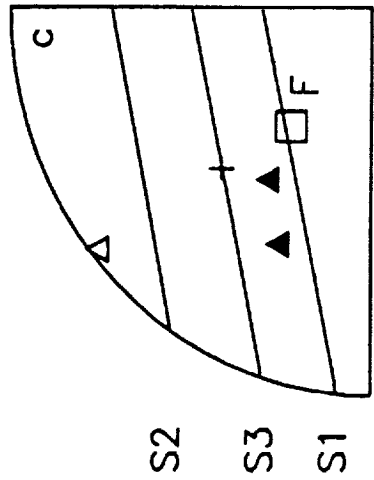
September 9,89   NRH

a   0:9:09:20–09:09:30
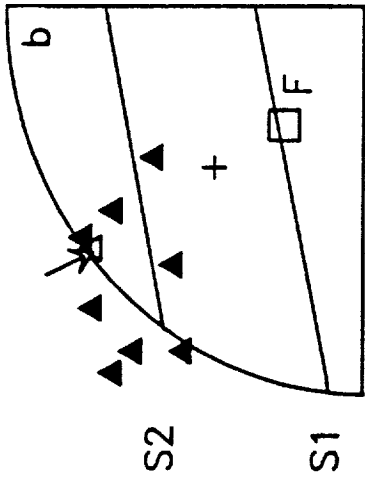
b   09:09:30–09:10:34

c   09:10:34–09:12:00
327 MHz and 164MHz

September 9,1989

SMM/GRS
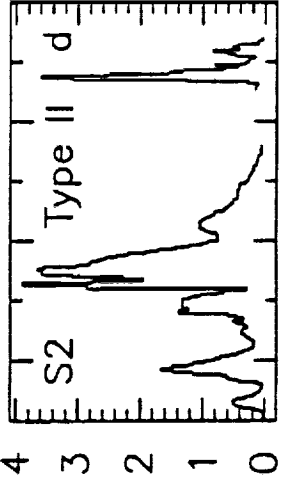114-199 keV

San Vito
4995 MHz

Nançay
435 MHz

Nançay
327 MHz

Counts s⁻¹

Flux (arbitrary units)

UT 9:09 9:10 9:11 9:12
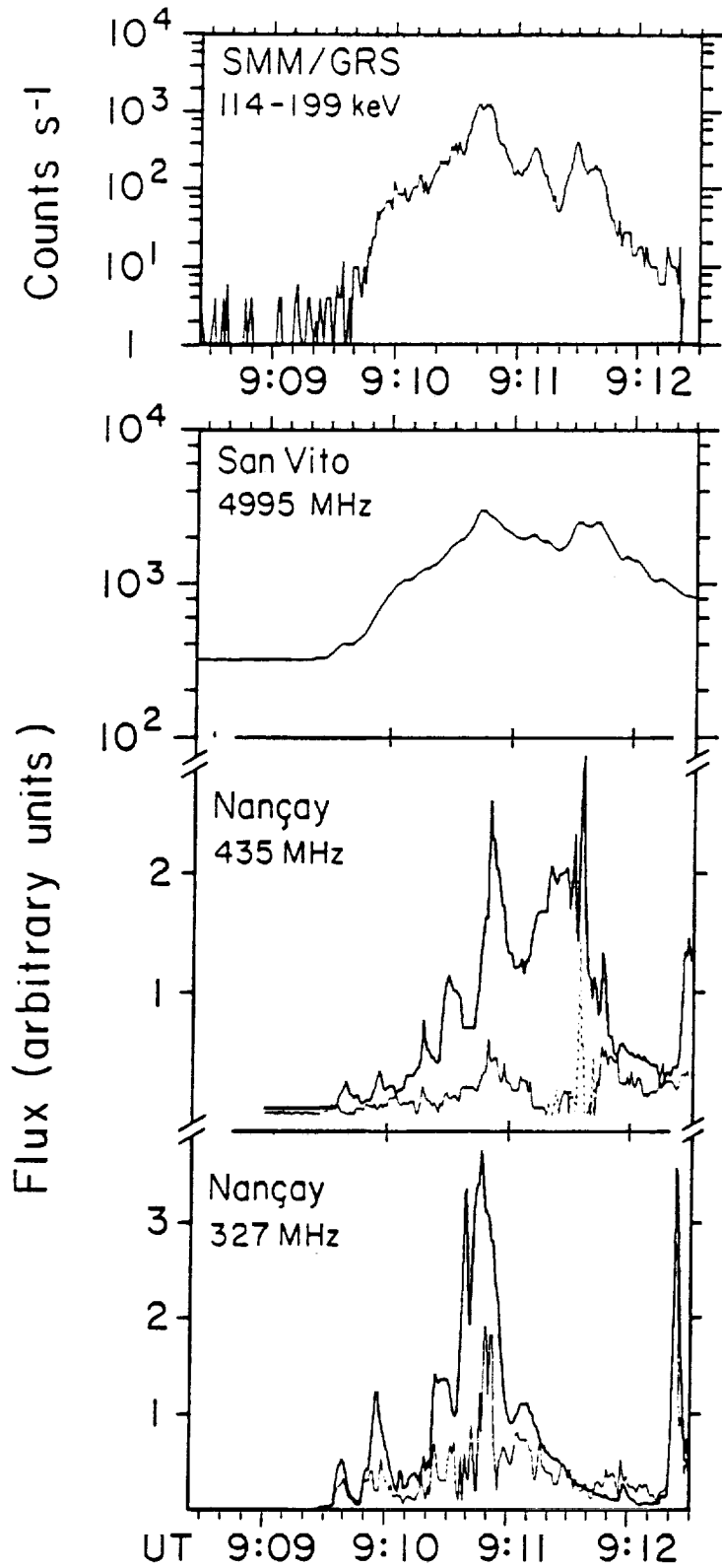
FIGURE 4

September 9, 1989

a — SMM/GRS — 4.1–6.4 MeV

b — 10–25 MeV

Counts (2s)$^{-1}$

c — NRH — 327 MHz — S3

d — Type II — S2

Flux (arbitrary units)
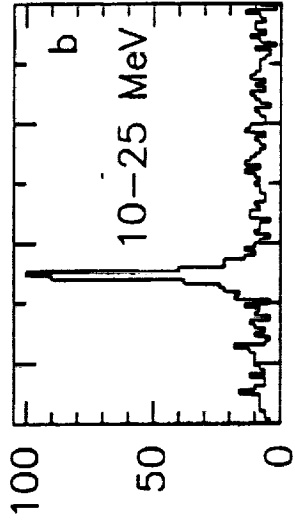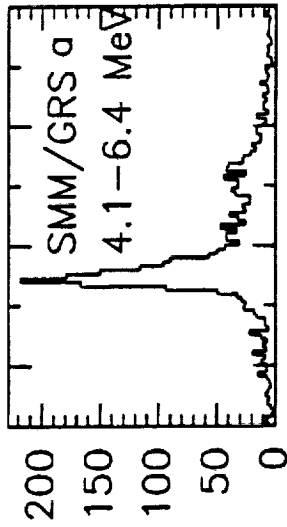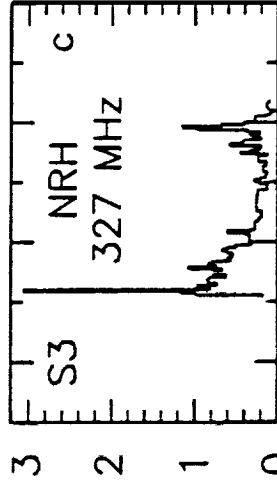
09:10   09:12   UT
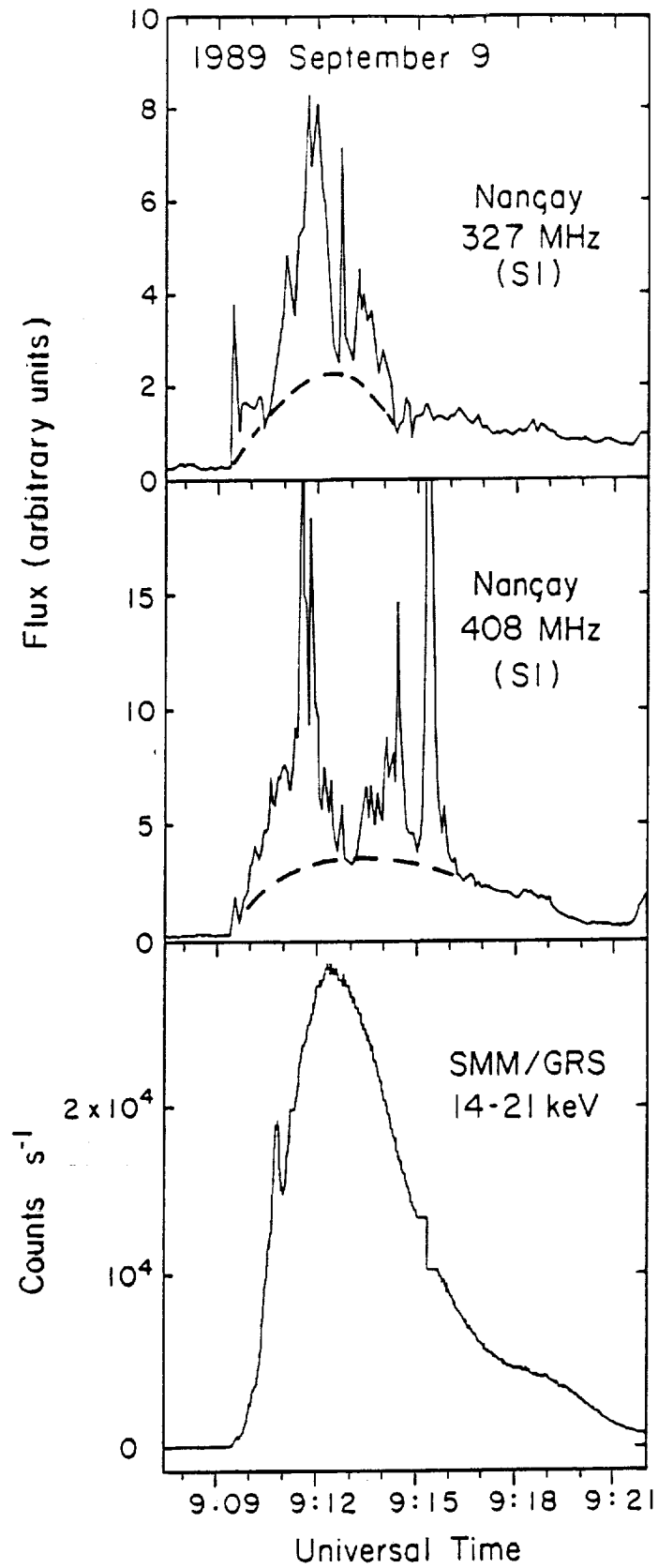
FIGURE 6

1989, SEPTEMBER 9

Hα − 0.5 A	Hα	Hα + 0.5 A
09:07:51	09:08:02	09:07:57
09:10:00	09:10:11	09:10:06
09:11:04	09:11:15	09:11:10
09:12:09	09:12:20	09:12:15

Figure E

Axis labels:
Counts MeV^{-1} (vertical axis)
Energy (Mev) (horizontal axis)

In-plot labels:
N-capture
e^+-e^-
^{24}Mg, ^{20}Ne....
^{20}Ne
^{12}C
^{16}O
lower curve: * 0.1

Phot. cm^{-2} MeV^{-1}

Energy (Mev)

FIGURE 9